New Evidence for TiO_2 Photocatalysis during Bilayer Lipid Peroxidation

J. Kiwi and V. Nadtochenko*

Laboratory of Photonics and Interfaces, Institute of Chemical Sciences and Engineering, Swiss Federal Institute of Technology (EPFL), Lausanne 1015, Switzerland

Received: April 20, 2004; In Final Form: July 30, 2004

The photocatalytic peroxidation of the bovine brain L-α-phosphatidyl-ethanolamine (PE) vesicle was measured and used as a model for phospholipid peroxidation. Synthetic phosphatidyl-ethanolamine, *E. coli* phosphatidyl-ethanolamine, lipid polysaccharide (LPS), and cardiopilin were used to compare the TiO_2 photocatalysis leading to cell wall membrane degradation. During the photocatalytic degradation, the appearance and growth kinetics were followed for (a) conjugated double bond formation, (b) malondialdehyde (MDA), (c) peroxides, and finally (d) the observed CO_2 evolution. Attenuated total reflection Fourier transform infrared spectroscopy (ATR-FTIR) was measured of PE bilayers cast on TiO_2 films and to a lesser extent for other phospholipids during TiO_2 photocatalysis. The decay kinetics induced by photocatalysis of the isolated cis C═C−H (3008 cm^{-1}), $-CH_2$, and $-CH_3$ groups and of the acyl-ester bond of the fatty acid in the glycerol backbone were followed in detail. The photocatalysis was also observed to induce spectral shifts in the CH_2 vibrations and changes in the asymmetric phosphate ester ($C-(PO_4)^--C$) stretching vibrations. The ATR-FTIR spectral changes suggest structural changes of the lipid bilayer due to peroxidation. The significant part of the photocatalytic peroxidation seems to take place at the TiO_2 surface by heterogeneous mediated processes. But concomitantly, a homogeneous chain radical peroxidation of PE occurs in aqueous solution by a radical chain mechanism.

Introduction

It has been known for over 20 years[1−4] that ionizing radiation such as X-rays, γ-rays, electrons, and α-particles, as well as UV-light, leads to free radical induced lipid peroxidation. Instability of lipids toward highly oxidative oxygen containing radicals leads to the degradation of biomembranes and has been the subject of many studies for nearly 50 years.[2−5] The increase in the lipid peroxidation (LPO) has been considered a common mechanism leading to the destruction of intracellular and cell wall membranes due to the cytotoxic products generated during the LPO process.[6−8] These LPO products are highly toxic in vivo and in vitro. They inactivate enzymes modifying their biomolecules and initiate free radical destruction of nucleic acids, proteins, and lipids. In living systems, the end products of lipid peroxidation exhibit mutagenic and carcinogenic properties.[2,3,6−8] In several studies TiO_2 films have shown bactericidal activity under UV light irradiation,[9−13] but the bactericidal function of TiO_2 photocatalysis is not well understood at the present time.

The objective of this work was the study of the lipid peroxidation due to the TiO_2 photocatalysis under UV-A light irradiation. The kinetics of the formation of the LPO products due to the peroxidation of the phosphatidyl-ethanolamine (PE) lipid layer on TiO_2 films was investigated. A lipid with the ethanolamine polar group was chosen as the model lipid because it is the main lipid present in the *E. coli* inner monolayer. A comparison with the LPO peroxidation kinetics of other cell wall lipid components is also reported in this study.

Experimental Section

Reagents. L-α-Phosphatidyl-ethanolamine (L-α-Cephaline) from bovine brain (Fluka); L-α-phosphatidyl-ethanolamine (L-α-Cephaline) Type V from *E. coli* (Sigma); dimiristoiyl phosphatidyl-ethanolamine (Fluka); lipid polysaccharide, LPS (Fluka); and Cardiolipin (Fluka). These reagents, acids, and bases were used as received.

TiO_2 Porous Membrane Preparation. A composite 8 μm thick film of TiO_2 (Degussa P25 (surface area 50 m^2/g) and poly(ethylene glycol) PEG-2000 (TiO_2 = 100 g/L and PEG-2000 30 g/L) was deposited in the form of a paste on a glass slide. The film was dried in air for 20 min. The PEG-2000 was mineralized at 400 °C for 30 min in an O_2 flow. No organic contamination was detected by ATR-FTIR on these TiO_2 porous films. The porous structure of the TiO_2 film was characterized by AFM microscopy.

Sample Irradiation. Samples were illuminated with four black (BL) Philips 18 W lamps emitting at 366 nm. A Suntest simulated sunlight irradiation chamber (Heraeus Noblelight AG, Hanau, Germany) with 95 mW/cm^2 was used in certain cases for comparative purposes.

Experimental Procedures. Semiconductor dispersions were prepared using TiO_2 (Degussa P25, 50 m^2/g). Spectrophotometric analyses of the irradiated solutions were carried out using a Hewlett-Packard 8452 diode-array spectrophotometer. The detection of peroxides in solution was carried out by the iodometric titration method, in which the I_3^- peak ($\epsilon = 26\,000$) is followed at $\lambda = 354$ nm.[14] CO_2 evolution in the irradiated samples was followed in a Carlo Erba 5300 GC equipped with a Poropak Q column in He at 120 °C.

Malondialdehyde (MDA) Determination. The thio-barbituric acid (TBA) method was used for photocolorometric measurements of malondialdehyde (MDA)[14] as modified by Anderson and Krinsky.[15] For calibration purposes, a solution of MDA was prepared by acid hydrolysis of 1,1,3,3-tetraethoxypropane according to Philpot.[5] An amount of 0.5 g TBA

10.1021/jp048281a CCC: $27.50
Published on Web 10/16/2004

SCHEME 1: Primary LPO Products Formed in the Lipid Peroxidation through ROO· in the Presence of O_2

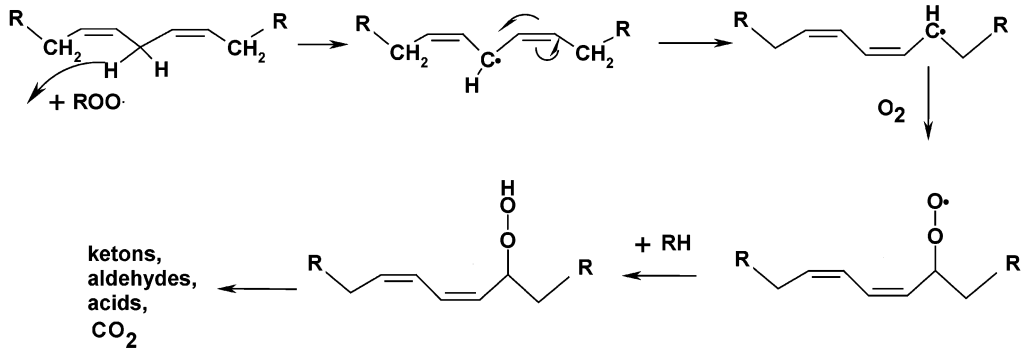

and 0.3 g sodium dodecyl sulfate (SDS) were dissolved in a 100 mL of aqueous solution using Millipore tri-distilled water. Solutions of the reagent were prepared immediately before analyses. Butylated hydroxy-toluene solution (BHT) was prepared by dissolving 0.22 g in 10 mL of absolute ethanol and stored at 4 °C. Ferric chloride solution was made with 0.27 g of ferric chloride dissolved in 100 mL of distilled water. It was stored in a screw-capped bottle at 4 °C. The MDA tests were carried out taking using 0.1 mL of a sample solution, 0.1 mL ferric chloride, 0.1 mL BHT, and 1.5 mL TBA reagents. The samples used were heated in boiling water in a fume hood for 15 min.

Spectrophotometric Determination of Conjugated Dienes. For evaluation of the formation of conjugated dienes, 100 μL of the liposome suspension was diluted in 1 mL of H_2O. The absorption spectra were measured in a 0.1 cm optical path length quartz cell. Conjugated dienes exhibit a distinct absorption in the UV at about 234 nm for the cis isomer (28 000 dm^3 mol^{-1} cm^{-1}) and at 236 nm for the trans isomer (26 000 dm^3 $mol^{-1}cm^{-1}$). The optical density at 234 nm was followed for the determination of the conjugated dienes.

Preparation of Lipid Samples for ATR-FTIR Spectroscopic Analyses. Three different approaches were used to detect by ATR-FTIR the LPO produced through TiO_2 photocatalysis. (i) Aliquots from the titania dispersions were withdrawn during irradiation at preselected times then deposited on the glass slide and dried. (ii) The PE films were cast on 8 μm porous TiO_2 membrane (Degussa P25). The PE was dissolved in a CH_3Cl/MeOH = 2:1 mixture and dried overnight in vacuum. Then the samples were immersed in distilled water and gently washed for 4 h under an argon atmosphere. The wet membranes loaded with PE were irradiated under BL light. (iii) The TiO_2 porous membrane (Degussa P25) was dipped in the small unilamellar vesicle (SUV) suspensions of PE. Then the loaded membranes were washed with tri-distilled water before irradiation. The SUV was prepared by the standard technique: (1) preparation of the thin dry film at the surface of the glass vessel; (2) transformation of the lipid film into the multilamellar vesicle suspension under N_2 atmosphere (concentration of 10 mg/mL); (3) ultrasonic treatment bath at 0 °C under Ar until the appearance of a transparent colloid. The techniques (ii) and (iii) showed better sample preparation reproducibility than when technique (i) was used. The ATR-FTIR spectra for wet TiO_2 porous membranes were measured on the samples that were vacuum dried overnight.

Fourier Transform Infrared Spectroscopy. ATR-FTIR spectra were measured in a Portmann Instruments AG spectrophotometer equipped with a Specac attachment (45° one pass diamond crystal). Spectra were the results of 256 scans with a resolution of 2 cm^{-1} in the spectral range 4000−5000 cm^{-1}. Fourier deconvolution procedures and spectra subtraction were carried out by a Win-IR Pro Bio-Rad software package. The resolution of the complex bands was performed by least-squares fitting with an IgorPro 4.08 program. The position of the IR peaks was found by the second or fourth derivative of the spectra and from the peak position in the spectra after Fourier deconvolution.

Control Experiments. Two types of control experiments were necessary during this study: (1) a lipid treatment in the air saturated solutions at room temperature in the TiO_2 dispersions in aqueous solutions and in the case of porous TiO_2 film for 4 h; (2) a lipid treatment under BL-light irradiation using nonsemiconducting Al_2O_3 instead of TiO_2. The porous film of Al_2O_3 was prepared in the same way as the TiO_2 film. During the control experiments, it was observed that the ATR-FTIR absorbance changes were negligible relative to the changes observed in the lipids irradiated in the presence of TiO_2 due to the significant peroxidation of the lipid samples The peroxidation indices (conjugated bonds, MDA, peroxides, CO_2) showed a narrow experimental variation during the reproduction of the experiments. Due to these observations, the background peroxidation of the lipids within the experimental time is not taken into account in this study.

Results and Discussion

Spectrophotometric Determination of Lipid Peroxidation Products. Lipid peroxidation is a complex process whereby an unsaturated lipid unit reacts with molecular oxygen to yield lipid hydroperoxide and dialkyl-peroxides (noted as LPO products in Scheme 1). To characterize these LPO products, different oxidation indices are used: (a) conjugated double bond formation, (b) formation of dialdehydes; (c) peroxide formation, and (d) production of CO_2.

The reaction of HO· or ROO· radicals with a polyunsaturated fatty lipid tail by the abstraction of an olefinic H-atom is a well-established process. After molecular rearrangement of L· (L = unsaturated chain in Scheme 1), the conjugation of double bonds takes place. The rearrangement of the double bonds leads to a stabilization of the lipid radical in the presence of O_2 and the formation of hydroperoxides occurs. When the lipid-acyl chain contains more than one double bond, lipid oxidation leads to the formation of the conjugated double bonds.

The changes in the absorbance profiles, noted as a rise in the absorption band at 234 nm in Figure 1, are proof that conjugated double bond formation took place during photocatalysis in the TiO_2 aqueous dispersion. From Figure 1, an estimation of the percentage lipid oxidation is possible. Using 22 000 M^{-1} cm^{-1} for the conjugated dienes and a PE molecular weight of 730, it is possible to estimate that one in about 50 lipid molecules

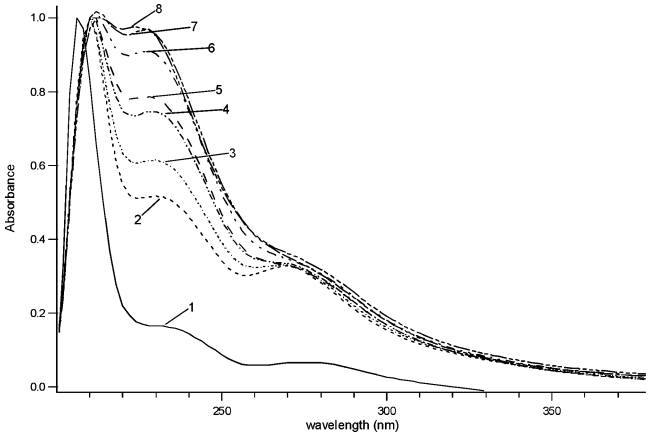

Figure 1. Spectral evidence of the conjugated double bond formation due to the photocatalytic peroxidation of PE in the TiO_2 dispersion. The spectra were normalized to the absorbance at 210 nm to show the rise of the conjugated double bonds in the system. [PE] = 1 mg/mL, [TiO_2] = 1 mg/mL, oxygen saturated solution, BL irradiation times: (1) zero min, (2) 14 min, (3) 28 min, (4) 43 min, (5) 61 min, (6) 95 min, (7) 141 min, (8) 206 min.

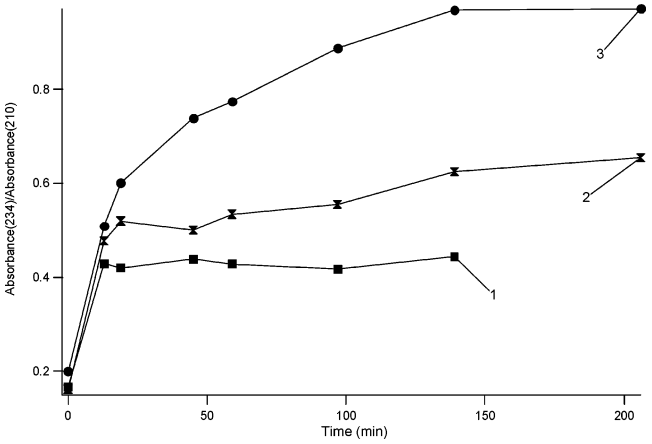

Figure 2. Kinetics of the conjugated double bond formation due to the photocatalytic peroxidation of PE in TiO_2 slurry under BL irradiation. [PE] = 1 mg/mL, [TiO_2] = 1 mg/mL. (1) Ar saturated solution, (2) air saturated solution, (3) oxygen saturated solution.

SCHEME 2: Conjugated Double Bond Formation Due to the Lipid Radical Formation on TiO_2 under Band Gap Irradiation

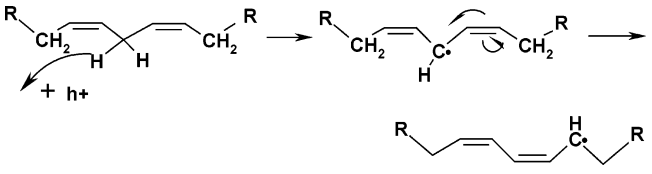

contain one conjugated diene. This estimation is based on the changes of absorption at λ = 234 nm and the amount of the lipid used.

Figure 2 shows the favorable effect of molecular oxygen on the kinetics of conjugated double bond formation. It was surprising to observe the formation of conjugated double bonds in an Ar atmosphere during the initial peroxidation stage. Figure 2 also shows that within 10 min, the rise of the conjugated double bonds in an Ar atmosphere is possible, but is ~30% less efficient than in O_2. A further rise in the conjugated double bond formation is observed in an O_2 atmosphere after 10 min of photocatalysis, whereas in an Ar atmosphere this formation did not proceed further. The formation of the conjugated double bounds in Ar atmosphere, the H-atom abstraction in fatty acyl chain, can be initiated by a hole generated on TiO_2 upon light irradiation. This is shown in the Scheme 2. In the presence of O_2, the mechanism in Scheme 1 seems to take place, leading to a higher conjugated double bond yield relative to the photocatalysis in an Ar atmosphere.

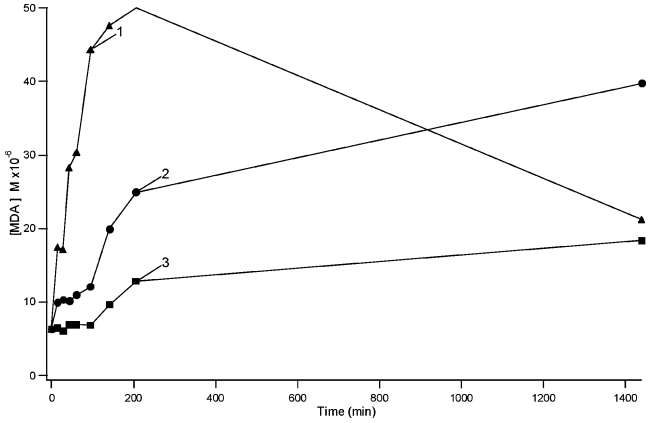

Figure 3. Kinetics of MDA formation due to the photocatalytic peroxidation of PE in TiO_2 slurries under BL illumination. [PE] = 1 mg/mL, [TiO_2] = 1 mg/mL. (1) Oxygen saturated solution, (2) air saturated solution, (3) Ar saturated solution.

MDA-like Product Formation. The kinetics of MDA product formation due to the photocatalytic peroxidation of PE during TiO_2 photocatalysis is shown in Figure 3. The measure of MDA is the absorbance of the colored product after the MDA treatment with TBA.[8] The TBA forms with MDA a pink complex at 532 nm with ϵ = 49 500 M^{-1} cm^{-1} linearly proportional to the lipid peroxidation of PE. The breakdown of hydroperoxides and lipid endoperoxide radicals leads to the formation of various products including malondialdehyde (MDA).[8,16] The most important observation reported in Figure 3 is that MDA species can be formed under Ar atmosphere. It means that, parallel to the mechanism shown in Scheme 3, an additional route for MDA formation exists without need for the presence of oxygen. In the presence of oxygen, the oxidation of the MDA reaches the highest value in Figure 3 after 200 min. Beyond 200 min, the PE oxidation seems to have been completed and the formation of MDA during PE degradation is no longer possible. The concentration of MDA decreases due to oxidation reactions. In air, the oxidation proceeds within a larger time scale. In an Ar atmosphere a decrease of MDA was not observed up to 55 h light irradiation.

Scheme 3 shows the path of MDA formation through intermediate endoperoxides.[1,6,16] Figure 4 shows the spectra for the color adducts of TBA with MDA for different lipids undergoing TiO_2-mediated photocatalysis. The difference in the spectra of colored adducts indicates that the photocatalytic peroxidation produces different MDA species (with a dialdehyde structure[8]) when photocatalyzing the degradation of different lipids. Oxygen was observed to favor higher MDA yield for four the lipids reported in Figure 4. The spectra reported in Figure 4 indicate that the intermediates during the oxidation process have a structure that is very close to the final oxidation product due to the similar spectral shapes observed as a function of time.

Figure 5 shows the kinetics of the peroxide formation for different lipids. The iodometric technique was used for this determination.[16] A comparison of peroxide formation for egg phosphatidyl-choline (PC), DMPE, and PE from *E. coli* indicates that for the egg PC lipid containing double bonds in the fatty

SCHEME 3: MDA Formation Due to the Monomolecular Chain Shortening of Endoperoxide Molecule

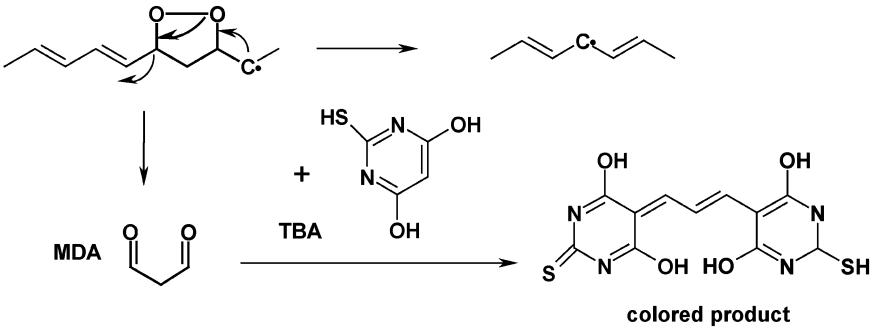

tails, the peroxide formation occurs faster than for DMPE or PE from *E. coli* that do not contain double bonds in the fatty tails.

Figure 6 shows the formation of the MDA-like products for different lipids. The kinetics in Figure 6 reports the absorbance changes observed at $\lambda = 532$ nm shown in Figure 4. The fatty tails of the different lipids contain a different number of the double bonds. PE from the *E. coli* has a lower double bond content than PE from the bovine brain. LPS and DMPE do not contain double bonds in the fatty tails. Figures 4 and 6 show the formation of MDA-like products. The Scheme 3 suggests a possible mechanism for the MDA-like product formation due to lipid peroxidation. In Scheme 3, the presence of double bonds is important and leads to the formation of MDA-like products. Figure 6 shows that the highest rate of MDA-like products comes from PE of bovine brain. This PE contains the highest number of double bonds, but MDA-like product formation is observed for the DMPE, which does not contain double bonds. Scheme 3 is not sufficient to explain the formation of MDA-like products due to photocatalytic peroxidation mediated by TiO_2, because the MDA product formation is observed in the absence of O_2. This implies that a significant part of the MDA-like products comes from the oxidation through TiO_2 photocatalysis and further hydrolysis of carbonium radicals not following the mechanism outlined in Scheme 3. Qualitatively, this suggestion is confirmed by the changes of pH observed during lipid peroxidation in O_2, air, and Ar atmospheres. PE samples at a starting pH 6.2 attain a pH of 5.5 after 2 h illumination in O_2, a pH of 4.5 in air, and a pH of 2.5 in Ar, respectively. The lipid radicals or ion-radicals formed due to TiO_2 photocatalysis can react with oxygen or hydrolyze in competitive reactions. In the absence of O_2, hydrolysis occurs lowering the solution pH. Lipid double bonds increase the yield of MDA-like products as suggested previously in Scheme 3.

Formation of CO_2. Figure 7 shows the kinetics of CO_2 formation due to the photocatalytic peroxidation. CO_2 molecules are not observed in the absence of O_2. It means that in the anaerobic conditions the mineralization of lipid is not possible. Taking the amount of CO_2 in Figure 7 and taking into consideration the M_w of PE of 730 and PE concentration of 1 mg/mL we can estimate that all the PE has been converted to CO_2 under O_2 atmosphere.

ATR-FTIR Spectroscopy of Lipid Peroxidation. The assignment of the ATR-FTIR bands of the PE is shown in Table 1. The lipid peroxidation due to TiO_2 photocatalysis causes

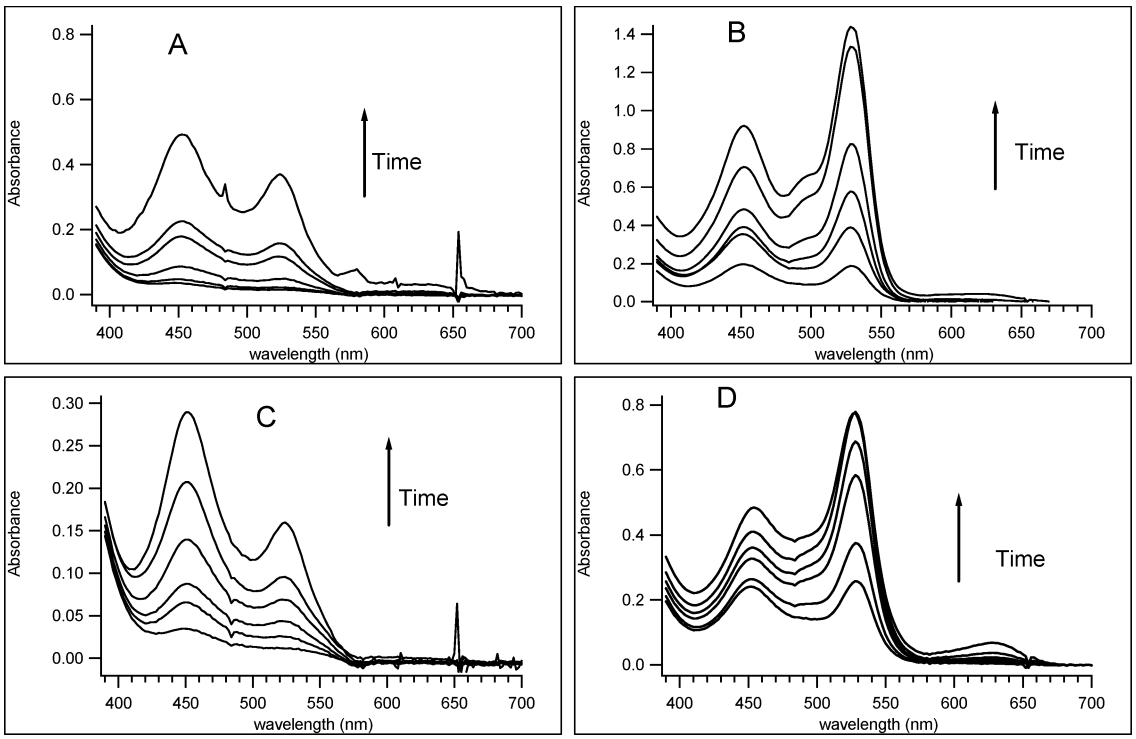

Figure 4. Spectra of the colored products in the presence of O_2 during MDA detection produced due to the peroxidation of the different lipids with TiO_2 under light irradiation: (A) DMPE, (B) Cardiopilin from bovine heart, (C) PE from *E. coli*, (D) PE from the bovine brain.

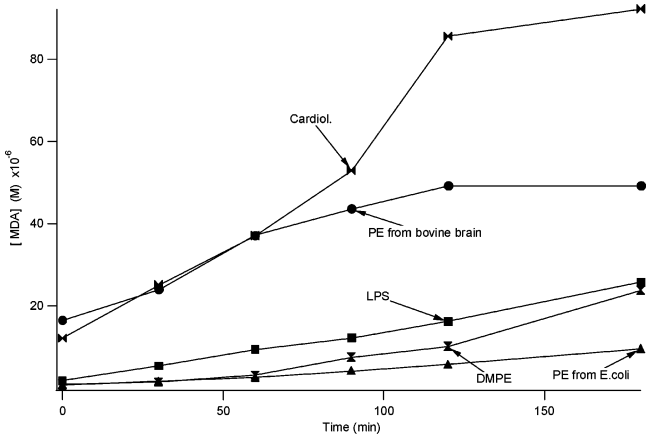

Figure 5. Kinetics of formation of MDA-like products due to the photocatalytic peroxidationat TiO_2 for different lipids in air. Lipids were used in the concentration 1 mg/mL. [TiO_2] = 1 mg/mL.

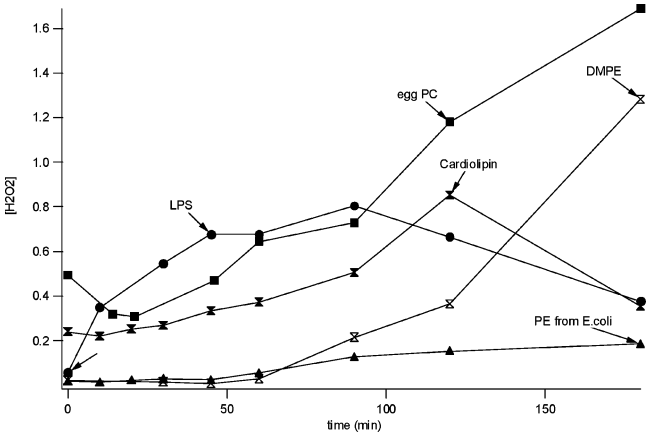

Figure 6. Kinetics of the peroxide formation determined by the iodometric technique. BL light was used. Concentration of the lipids used was 1 mg/mL. Air saturated solution. [TiO_2] = 1 mg/mL.

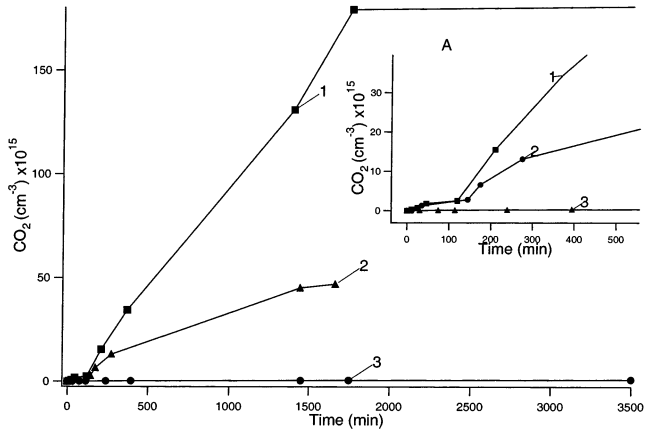

Figure 7. Kinetics of CO_2 formation during the photocatalytic peroxidation of PE under BL illumination. [PE] = 1 mg/mL, [TiO_2] = 1 mg/mL. (1) Oxygen saturated solution, (2) air saturated solution, (3) Ar saturated solution. The inset A shows the CO_2 formation for the same reaction during the initial reaction stages. [PE] = 1 mg/mL, [TiO_2] = 1 mg/mL.

changes in the vibrational spectral bands in the wet PE vesicle films as well as in multilamellar PE films on TiO_2 porous membranes. The changes in the ATR-FTIR absorption spectra of PE before and after different irradiation times on wet TiO_2 films are shown in Figure 8. The spectral modifications of the C−H stretching vibrations relate to the peaks are shown in Figure 8.

TABLE 1: Assignment of the C−H Spectral Vibration Bands Shown in Figures 8A and 8B

wave-number	band	assignment	ref
3007.06	ν_a(CH)	cis C═C−H	2;16;17
2959.1	ν_a(CH_3)	C−CH_3	2;16−18
2919.58	ν_a(CH_2)	(CH_2)*n*	2;16−18
2872.96	ν_a(CH_3)		16;17
2850.72	ν_s(CH_2)	(CH_2)*n*	2;16−18
1740.74	ν(C═O)		19;20
1466.09	δ(CH_2)n	(CH_2)*n* scissoring, lipid chain	2;16;20
1411.9	δ(α-CH_2)	CH_2−COOC	2;20;21
1376.54	δ(CH_3)	C−CH_3	2;16;21
1342.57	γ_w(CH_2)	(CH_2)*n*	2
1316.92	γ_w(CH_2)	(CH_2)*n*	2;22
1292.42	γ_w(CH_2)	(CH_2)*n*	22
1269.19	γ_w(CH_2)	(CH_2)*n*	22
	1260 ν_a(P═O)	C−(PO_4^-)−C	2
1243.31	γ_w(CH_2)	(CH_2)*n*	22
1220.09	γ_w(CH_2)	(CH_2)*n*	22
1170.52	ν(C−O)	CH_2−COOC	2
	1170.9	ytCHz and ywCH2 parallel to the hydrocarbon chain	20
1119.79	1109.1	ν_s(P═O) in line with P−O bond	20
1088.71	1097	ν_s(P═O) in line with P−O bond	20
	1092, 1090	P−C (C−OPO3−C)	2;23
1060.75	1061.8	ν_s(PO_2) parallel to the bisector of the O−P−O angle	20
		1061 naC−C (acyl chain, trans conformers, ttt)	24
		1040−910 î(PO) in POH	21
995.81	995.3	ν_a(P−O) antisymmetric P−O single bond stretch	20
969.58	1050−970	ν(POC)	21

The main observations relating to the spectral changes observed in Figure 8 can be summarized as follows. (1) In the spectral region of the OH-bond absorption (3500−3000 cm^{-1}), a change in the profile and intensity of the peaks can be readily seen in Figure 8a. Due to the water absorbed on the PE/TiO_2 film moiety under light irradiation, peroxides, alcohols, and carboxylic groups are formed and new OH-bonds are produced due to these functional groups. (2) At 3008 cm^{-1} a decrease of the intensity of the ν_a(CH) band is noticed corresponding to the isolated cis C═C−H stretching vibration. This decrease relates to the decay kinetics of the isolated double bonds in the lipid. The decay of the absorbance of the bands −CH_2 (2920 cm^{-1}, 2850 cm^{-1}) and −CH_3 (2960 cm^{-1}, 2870 cm^{-1}) is also observed. This is due to −C−H bond peroxidation. The concomitant decrease of the −CH_2 and −CH_3 band intensity shows that −CH_2 and −CH_3 groups were susceptible to peroxidation. The shift in the peak position of the −CH_2 vibrations is proof that a structural transformation occurred in the lipid layers. (3) In the fingerprint spectral region 1900−750 cm^{-1} (Figure 8b), changes of the absorption profile were observed along with changes in the region of the carbonyl group absorption between 1750 and 1500 cm^{-1}. A decrease of the −CH_2 absorption band at 1467 cm^{-1} was also detected. The appearance of a wide absorption between 1300 and 900 cm^{-1} was observed in parallel to the decrease of the intensity of the PO_2 vibrations found in the 1200−900 cm^{-1} region. The total intensity of the absorption in the 1900−750 cm^{-1} region was also observed to decrease with irradiation time.

Spectral Integral Decay. Figure 9 shows the decay due to the photocatalytic peroxidation on the TiO_2 films of the integral of the bands from the different spectral regions of PE by ATR-FTIR. The integral analysis is a characteristic of the total absorbance for each of the bonds investigated. The integrals for the wide spectral region can be used for the rough estimation

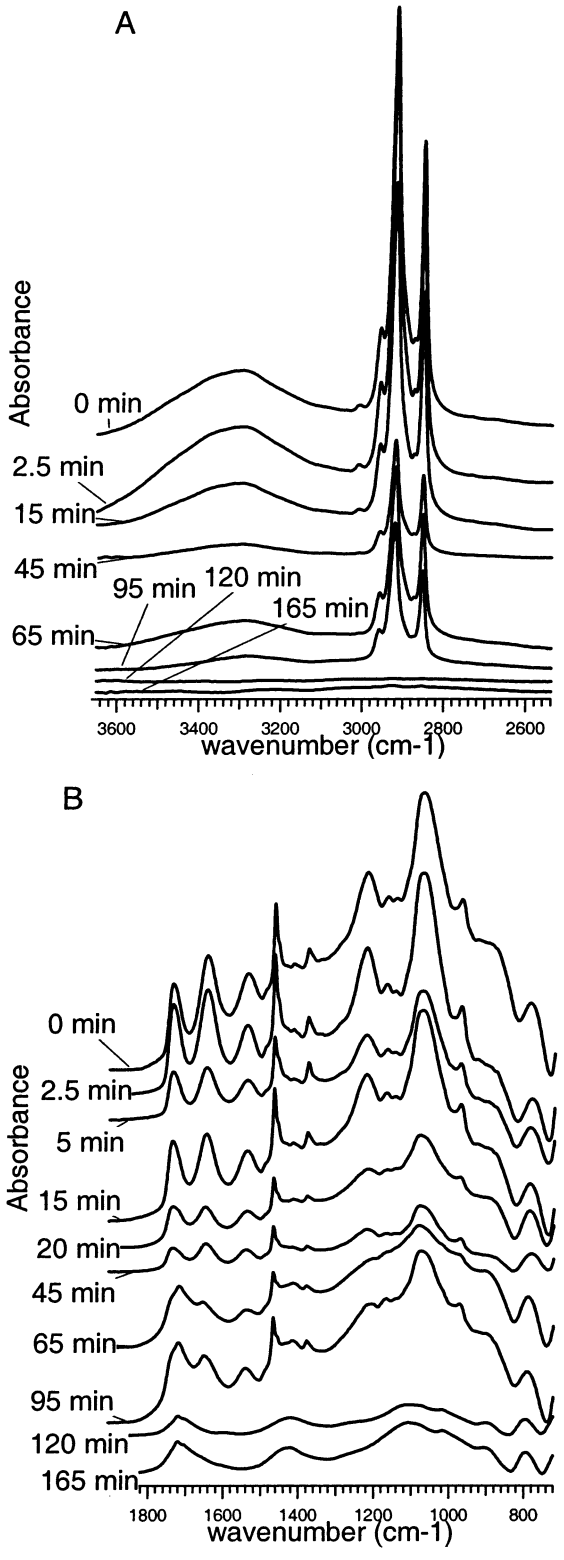

Figure 8. Changes of the spectral profiles of bovine brain PE due to the photocatalytic oxidation at TiO_2 porous films. The absorption of the pure TiO_2 porous film was subtracted in each case. The exposition time is indicated in the labels to the figure.

of the total amount of the lipid and peroxidation products on TiO_2, assuming that the integrals of the oscillator strength of the initial compound, the intermediates, and the terminal products stay fairly stable during the integration in the wide spectral region.

Integrals of the absorbance bands in Figure 9 were obtained and analyzed for the wax region of the absorption of $-CH_3$ and $-CH_2$ bands plus cis C═C−H at 3008 cm^{-1} (in the spectral window 3130−2580 cm^{-1} in Figure 9A), the cis C═C−H around 3008 cm^{-1} (Figure 9B), the spectral region 1800−900 cm^{-1} (Figure 9C), and the spectral region of the C═O group absorption between 1774 and 1700 cm^{-1} (Figure 9D). The decay of the cis C═C−H occurs faster than the decay of the $-CH_3$ and $-CH_2$ bands in the wax region. The decay time for (HC═CH_2−) is $1/\tau_{C=C} = 0.105 \pm 0.04$ min^{-1}. About the same decay time was obtained for the decay ratio of the integral of the cis C═C−H absorbance to the integral of the absorbance of $-CH_3$ and $-CH_2$ bands in addition to the cis C═C−H band. The value obtained of $1/\tau_R = 0.08 \pm 0.03$ min^{-1} coincides within the error limit with $1/\tau_{-C=C-H} = 0.105-0.04$ min^{-1}. The weakest bond −C═C−H was observed to undergo peroxidation in the shortest time.

The decays of the $-CH_3$ and $-CH_2$ band integrals show a slower decay between 1774 and 1700 cm^{-1} (Figure 9D). The approximation of this curve by double exponential decay gave the following values: wax region A1/(A1+A2) = 0.49, $1/\tau_1 = 0.0077$ min^{-1}, $1/\tau_2 = 0.16$ min^{-1}; fingerprint A1/(A1+A2) = 0.47, $1/\tau_1 = 0.007$ min^{-1}, $1/\tau_2 = 0.16$ min^{-1}; for the absorption from the C═O bonds 1770−1700 cm^{-1} A1/(A1+A2) = 0.38, $1/\tau_1 = 0.0034$ min^{-1}, $1/\tau_2 = 0.097$ min^{-1}. The similar values found for the decay parameters indicate that the decrease of the integral absorbance for the wax, fingerprint, and C═O bond regions is due to losses of the lipid peroxidation being mineralized to CO_2. After abstraction of the double allyl H-atom, molecular rearrangements lead to the conjugation of the double bonds during the early reaction stages during photocatalytic peroxidation (Scheme 1). At this stage of the reaction, the cis C═C−H bond is not isolated anymore and hence does not contribute to the absorption at 3008 cm^{-1}. Thus, the absorption band at 3008 cm^{-1} seems to be involved in the early peroxidation stages.

Peroxidation Intermediates Detected by ATR-FTIR. In Figure 10, the well-known Fourier deconvolution procedure of the spectral profile was used to enhance the resolution of the overlapping bands. Figure 11 shows the plot of the second derivative spectral profiles. This procedure also allows further discrimination of overlapping peaks. From Figures 8, 10, and 11, the characteristic region of the C═O bond spectral region can be seen between 1800 and 1500 cm^{-1}. We observe a consistent increase in the absorption bands at 1720, 1716, 1703, 1697, 1694, 1683, 1656, 1645, and 1635 cm^{-1} in the C═O stretching region of the α,β unsaturated aldehydes formed during the breakdown of hydroperoxides or lipid endoperoxides. Some examples: hexanal has a band ν(RHC═O) at 1726 cm^{-1}; hexenal has a band ν(RHC═O) at 1697 cm^{-1}; 2,4-decandienal has a band ν(RC═CH−HC═O) at 1689 cm^{-1} and a band ν(RC═CH−HC═O) at 1642 cm^{-1}; 4-hexen-3-one has bands ν(RC(═O)HC═CHR) at 1703 and 1679 cm^{-1} and ν(RC(═O)-HC═CHR) at 1635 cm^{-1}, and oleic acid RC(═O)OH at 1711 cm^{-1}.[25] As can be seen from Figures 8, 10, and 11, the intensity of aldehydes and carboxy acid bands was a function of the irradiation time due to the variation observed in the amount of the peroxides produced.

Figures 8, 10, and 11 show that the absorbance band at 1744 cm^{-1} is attributed to the C═O vibrations of the acyl bond. The absorbance of the lyso-phospholipids has been reported at 1726 cm^{-1} and was observed to have a bandwidth of 29 cm^{-1}, whereas the bandwidth of the fatty acid monomers at 1726 cm^{-1} has a bandwidth of 50 cm^{-1}. Carboxylate anions were observed at 1680 cm^{-1} with a bandwidth of 23.5 cm^{-1}. As reported in Figures 10 and 11, the bands of the acyl C═O vibrations

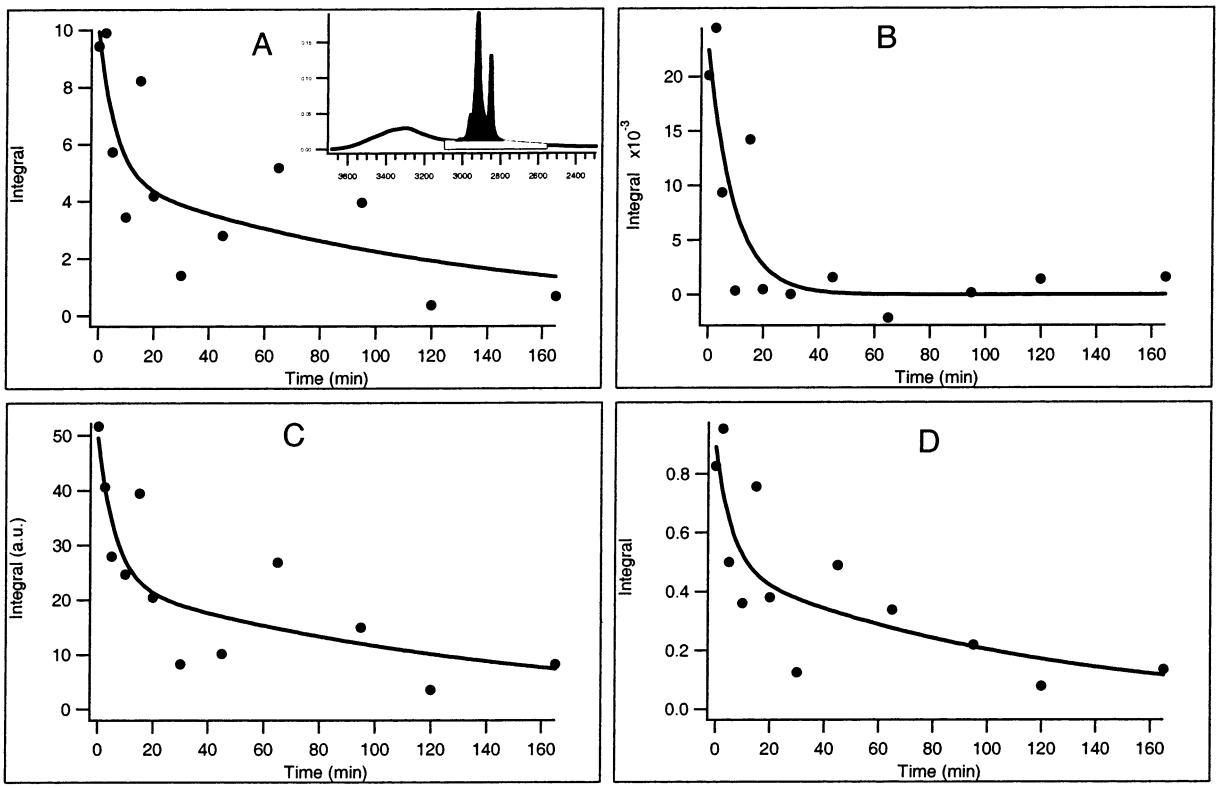

Figure 9. Decay of the integrals from different regions of the ATR-FTIR spectra of PE during photocatalytic peroxidation at TiO_2. (A) $-CH_3$ and $-CH_2$ peaks. Integration limits: 3130−2580 cm^{-1}. Inset A shows in the filled area the integration area. (B) Double bond peak around 3008 cm^{-1}. Integration limits: 3030−2950 cm^{-1}. (C) Complete fingerprint region. Integration limits: 1800−900 cm^{-1}. (D) Carbonyl bounds region. Integration limits: 1774−1700 cm^{-1}.

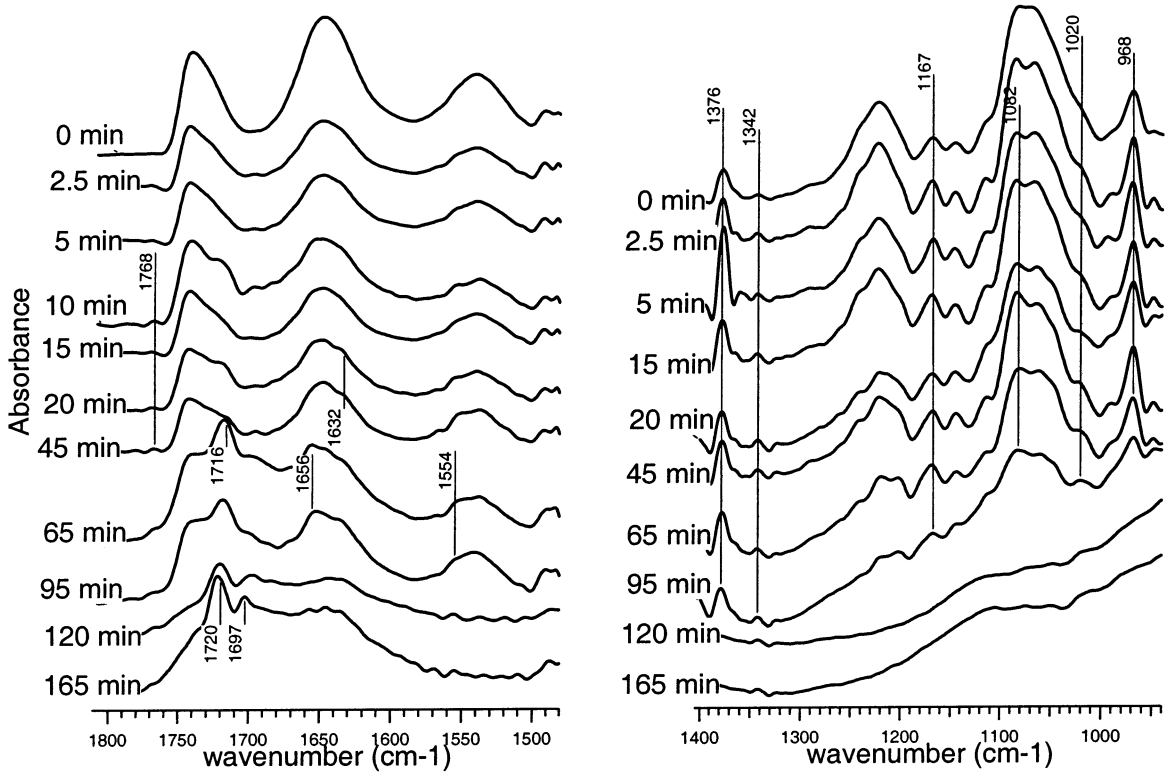

Figure 10. Changes of the absorption profiles in the deconvoluted Fourier spectra. Deconvolution parameter $K = 2.274$ (K is defined as the effective increase in deconvolution), half width = 8 cm^{-1}. The spectral profiles were normalized for the maxima in the spectral region under observation.

disappear before any other band due to at TiO_2 photoactalysis. The rise of the absorbance at 1726 cm^{-1} is observed in Figure 11, contributing to the widening of the peak at 1744 cm^{-1}.

Further evidence for the structural modifications introduced during the photocatalysis in PE can be found in Figure 11 in the spectral region between 1500 and 1300 cm^{-1} and in the

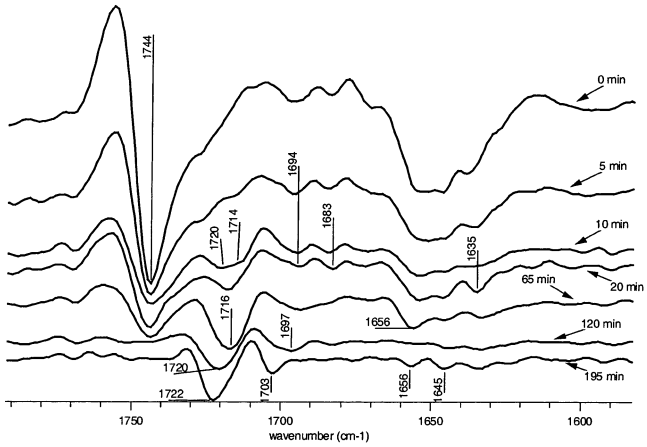

Figure 11. ATR-FTIR spectra of PE due to the photocatalytical oxidation at the porous film of TiO_2. Data are presented in the form of the second derivatives. The times of irradiation are indicated on the figure.

spectral region between 2800 and 3000 cm^{-1}. The asymmetric bending vibration of the $-C-CH_3$ group at 1457 cm^{-1} decreased in intensity upon irradiation, indicating that the fatty acid tails did also get the effect of the photocatalytic radical induced chain reaction. The asymmetric $\nu_a(CH_2) = 2920$ cm^{-1} and the symmetric $\nu_s(CH_2) = 2850$ cm^{-1} $-CH_2$ stretching vibrations, which are sensitive to the conformation of the fatty acid chains, were observed to shift to a higher frequencies upon light irradiation.

Spectral Shift Detection of the Structural Modifications of the PE Bilayers. Figure 12 shows the spectral shifts of the peaks as a function of irradiation time for membrane PE moieties on porous TiO_2 films. This shift was observed for the samples of lipid films on TiO_2 porous membrane and for the SUV vesicles cast on the TiO_2 porous membrane. Recently it has been found by AFM in our laboratory[27] that the SUV vesicles remained intact on the TiO_2 films in the dark for periods above 2 h.

Figure 13 shows the linear correlation of the peaks shift reported in Figure 12 as a function of irradiation time. The observed shift suggest an increase in microviscosity during the TiO_2 photocatalysis. The shift of the peak is more pronounced for the PE films on TiO_2 dehydrated in vacuum. In Figures 12 and 13, the experimental data have been obtained with films dried in this way to avoid the effect of the humidity on the spectra during ATR-FTIR analysis. For the wet films, the amplitude of the shift taken as the difference between the position of the peak maximum at time zero and after 1 h irradiation was ~1.5 times lower than for the same samples after drying. The maximum amplitude of the shift was ~2 times lower for the SUV PE on TiO_2 porous films compared to the shifts found for PE films on TiO_2.

Figure 14 shows the difference of the $-CH_2$ peaks of PE depending on the form of the PE organization. The positions of the $-CH_2$ peaks were sensitive to the structural organization of the PE. This difference refers to the following bands: scissoring vibrations of $-CH_2$ at 1467 cm^{-1}, the end-group methyl vibrations at 1457 cm^{-1}, the shift observed for the $-CH_2$ stretching vibrations, and finally the shift of the phosphonic vibrations near 1100 cm^{-1} (not shown in Figure 14).

The spectral shifts involving $-CH_2$ groups have been recently reported[27] to be associated with an increase in the lipid bilayer fluidity reflecting changes in the bilayer structure. The results shown in Figure 14 allows us to state the following observations. (a) The adsorption of the PE lipid on TiO_2 in the form of the lipid multibilayer films and in the form of the vesicles disturbs the spectra of PE. The photocatalytic peroxidation induced spectral changes that reflect PE structural modifications. (b) The sample humidity affects the PE spectral profiles and consequently the observed structural modifications.

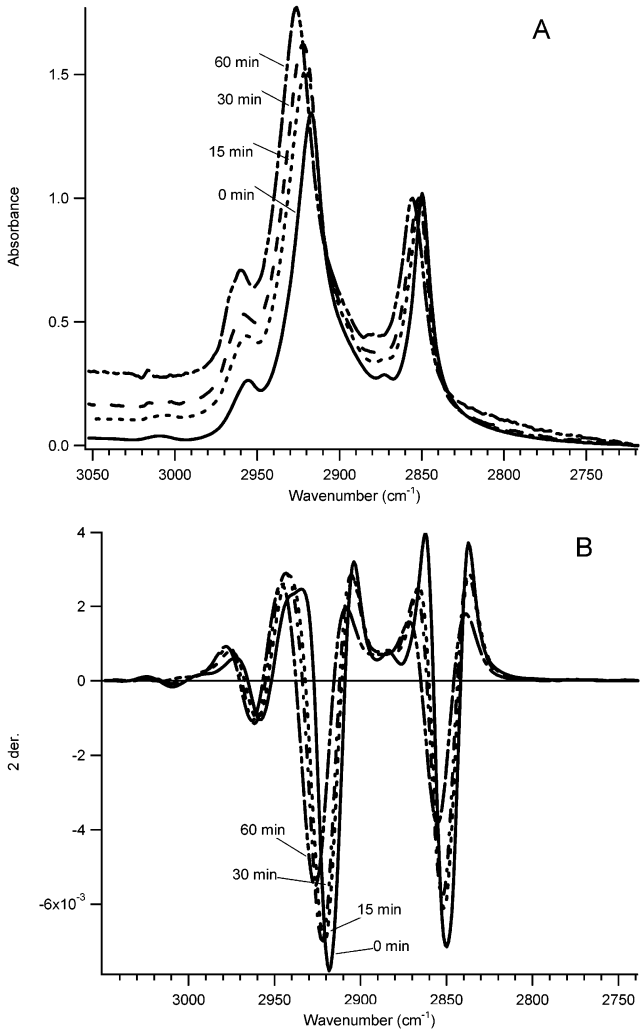

Figure 12. Shift of the PE $-CH_2$ and $-CH_3$ peaks due to the photocatalytic peroxidation at TiO_2 porous film. PE cast on TiO_2 films. Dried samples. (A) Spectral profiles of $-CH_2$ and $-CH_3$ bands. (B) Second derivatives of the spectra. Irradiation by BL light.

The radical−radical[1,10,16] reactions due to TiO_2 photocatalysis account for the spectral changes observed in the PE upon irradiation. An increase in the cross linking mobility of the fatty acid leading to structural modifications in the PE multibilayer packing would be the reason for the spectral changes. Lipid peroxidation leads to chemical modifications such as the formation of polar substances such as hydroperoxides, aldehydes, and carbonic acids.[1,6,16,27] The increased polarity of the fatty acid chains due to the formation of hydroperoxides has been reported to induce an increase in the distance between the adjacent fatty acid chains.[26] This in turn leads to an increase of the intermolecular distances explaining the shift observed for the phosphate−ester vibrations.

Figure 15 shows the spectral profiles changes for the PE film cast on TiO_2 after photocatalytic peroxidation. The samples were dried before the ATR-FTIR measurements, and the observed changes agree with the results obtained in Figures 8 and 10 for wet samples. Drying of the samples avoids the effect of hydration on the phosphonic bands. Photocatalysis induced changes of the asymmetric phosphate ester (C−(PO_4)−C)

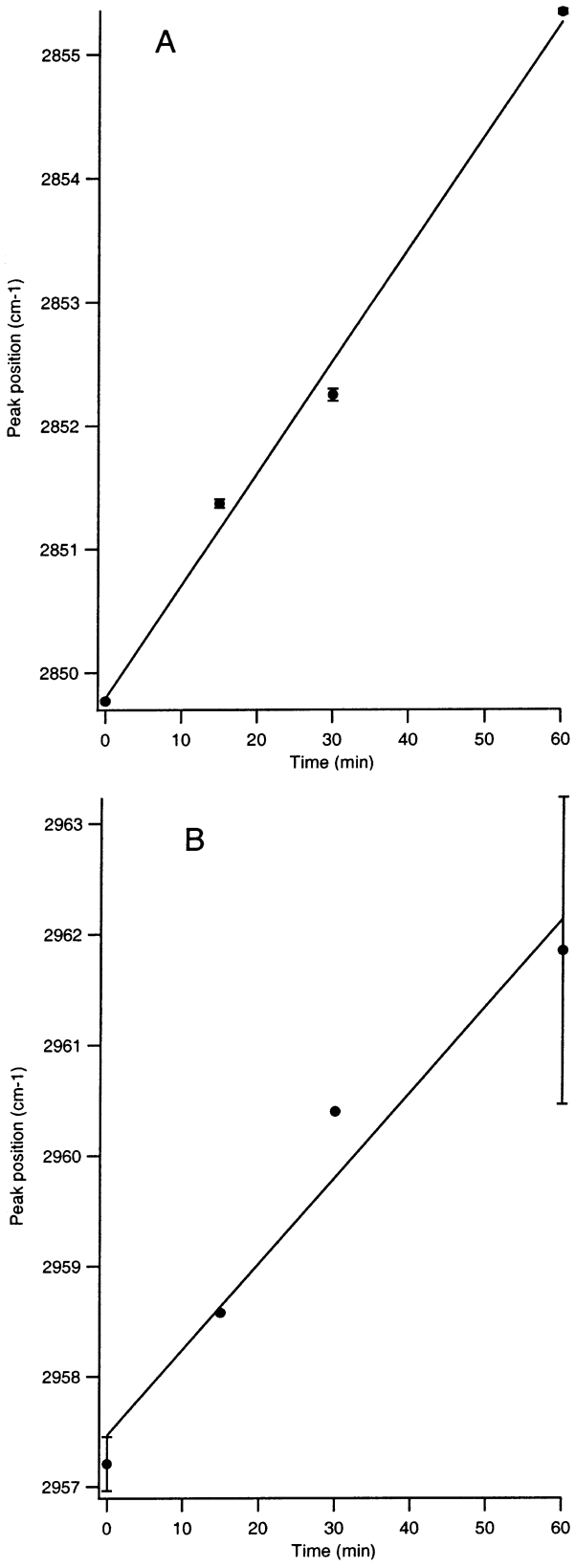

Figure 13. Dependence of the peak of $-CH_2$ bands as a function of time. (A) Dependence of the $\nu_a(CH_2)$ band vs time. (B) Dependence of the $\nu_s(CH_2)$ band vs time.

stretching vibrations (ν_a(P═O)) and changes related to modifications of the fatty acid chains caused by double bond conjugation or peroxidation. The latter chemical changes modify the packing of the lipid layers accounting for the observed spectral changes.

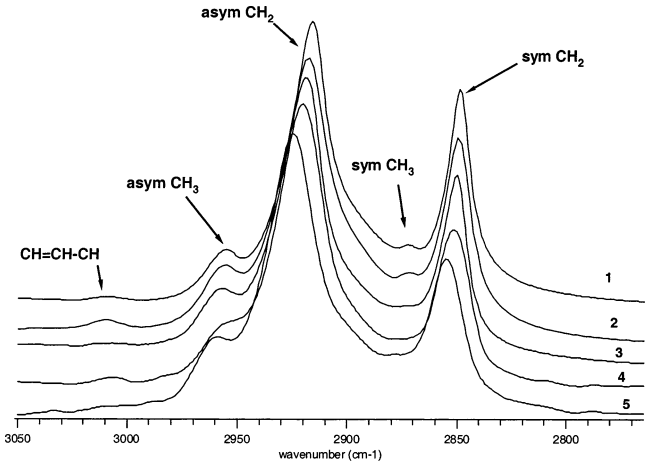

Figure 14. Spectral profiles of the PE lipid in different organization of lipid layers. (1) Dry PE film at TiO_2: $\nu_a(CH_3)$ 2955.29 cm^{-1}, $\nu_a(CH_2)$ 2916.37 cm^{-1}, $\nu_s(CH_3)$ 2872.57 cm^{-1}, $\nu_s(CH_2)$2849.65 cm^{-1}. (2) Dry PE film at glass: $\nu_a(CH_3)$ 2955.85 cm^{-1}, $\nu_a(CH_2)$ 2917.71 cm^{-1}, $\nu_s(CH_3)$ 2872.93 cm^{-1}, $\nu_s(CH_2)$ 2850.11 cm^{-1}. (3) Wet PE TiO_2 film: $\nu_a(CH_3)$ 2957.5 cm^{-1}, $\nu_a(CH_2)$ 2917.65 cm^{-1} , $\nu_s(CH_3)$ 2873.52 cm^{-1}, $\nu_s(CH_2)$ 2850.48 cm^{-1}. (4) SUV of PE in water: $\nu_a(CH_3)$ 2956.67 cm^{-1}, $\nu_a(CH_2)$ 2920.96 cm^{-1}, $\nu_s(CH_3)$ 2876.4 cm^{-1}, $\nu_s(CH_2)$ 2851.9 cm^{-1}. (5) SUV PE at TiO_2: $\nu_a(CH_3)$ 2960.53 cm^{-1}, $\nu_a(CH_2)$ 2925.35 cm^{-1}, $\nu_s(CH_3)$ 2878.99 cm^{-1}, $\nu_s(CH_2)$ 2854.88 cm^{-1}.

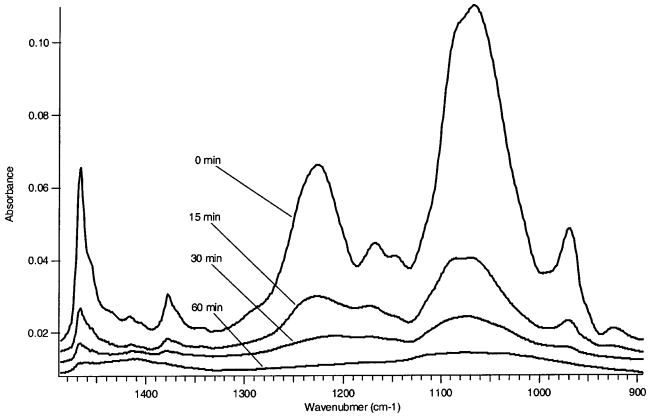

Figure 15. Spectral profile changes, of the PE lipid film cast on TiO_2 porous membrane during photocatalytic peroxidation. The samples after the photocatalytic treatment were dried in vacuum overnight.

Conclusions

1. Peroxidation due to the PE photocatalysis on TiO_2 has been followed by spectroscopic techniques. This study reports (a) formation of the conjugated double bonds in the fatty chains, (b) MDA formation, (c) peroxide formation, and (d) CO_2 formation. The evolution of CO_2 by PE upon TiO_2 photocatalysis was observed only in the presence of O_2. The presence of double bonds in the fatty chains in the lipids and oxygen were favorable factors leading to lipid mineralization in addition to lipid peroxidation. This is in agreement with the chain radical reaction theory for the peroxidation of lipids.

2. The ATR-FTIR spectral shifts of the symmetrical $\nu_s(CH_2)$ near 2850 cm^{-1} and asymmetrical $\nu_a(CH_2)$ near 2920 cm^{-1} suggest changes in the lipid bilayer structure event at the initial stages of peroxidation. The blue shift of these bands indicates the increase of fluidity in the fatty tail region. The changes of the band shapes found for the phosphonic groups near 1260 cm^{-1} provide the additional evidence for the structural modifications in the lipid bilayer.

3. During this study was found that (a) formation of peroxides occurs faster for lipids containing double bonds in the fatty tails;

(b) MDA-like products are formed both in the lipid with the double bonds in the tails and in the lipids without double bonds in the tail. However, the MDA formation from the lipids with double bonds is faster than from the lipids without double bonds; (c) MDA-like products are formed in anaerobic conditions; (d) a shift to more acidic pH values is observed in the absence of oxygen. The redox process at the TiO_2 interface leads to two types of reactions: (a) the initiation of a chain radical oxidation in the presence of O_2 and (b) to a heterogeneous oxidation of lipids that can eventually proceed in the absence of O_2 with the formation of the MDA-like products in the anaerobic conditions.

4. ATR-FTIR spectroscopy detects the disappearance of the single double bonds at the 3008 cm^{-1} band by following the $-C{=}C-CH_2$ vibrations. The formation of aldehydes and carbonic acids can also be detected by ATR-FTIR. The destruction of the acyl bond between the fatty acid and glycerol at the initial stages of the photocatalysis was identified. The peroxidation mediated by theTiO_2 photocatalysis induces spectral shifts in the $-CH_2$ vibrations that are sensitive to the structural modifications of the lipid layers. The transformation of the asymmetric phosphate ester $C-(PO_4)-C$ stretching vibration ($\nu_a(P{=}O)$) seems to be proof for the lipid modification upon TiO_2 photocatalysis.

Acknowledgment. This work was financed by Grants of CTI TOP-NANO 21 No. 5897.5 and OFES COST 19 No. CO2.0068, both from Bern, Switzerland, and INTAS 00-0554.

References and Notes

(1) Chartterjee, S. N.; Agarwal, S. *Free Radical Biol. Med.* **1988**, *4*, 51−72.

(2) Kinder, R.; Ziegler, C.; Wessels, J. M. *Int. J. Radiat. Biol.* **1997**, *71*, 561−571.

(3) Moore, D. J.; Sillis, R. H.; Mendelsohn, R. *Biospectroscopy* **1995**, *1*, 133−140.

(4) Mandal, T. K.; Chartterjee, S. N. *Radiat. Res.* **1980**, *83*, 290−302.

(5) Philpot, J. ST. L. *Radiat. Res. Suppl.* **1963**, *3*, 55−70.

(6) Hemmingsen, A.; Allen, J. T.; Zhang, S. F.; Mortensen, J.; Spiteri, M. A. *Free Radical Res.* **1999**, *31*, 437−448.

(7) Lamba, O. P.; Lal, S.; Yappert, M. C.; Lou, M. F.; Borchman, D. *Biochim. Biophys. Acta* **1991**, *1081*, 181−187.

(8) Maness, P. C.; Smolinski, S.; Blake, D. M.; Huang, Z.; Wolfrum, E. J.; Jacoby, W. A. *Appl. Env. Microbiol.* **1999**, *65*, 4094−4098.

(9) Kasaikina, O. T.; Kortenska, V. D.; Kartasheva, Z. S.; Kuznetsova, G. M.; Maximova, T. V.; Sirota, T. V.; Yanishlieva, N. V. *Colloids Surf. A* **1999**, *149*, 29−38.

(10) Wolfrum, E. J.; Huang, J.; Blake, D. M.; Maness, P. C.; Huang, Z.; Fiest, J.; Jacoby, W. A. *Environ. Sci. Technol.* **2002**, *36*, 3412−3419.

(11) Sahai, N. *J. Colloid Interface Sci.* **2002**, *252*, 309−319.

(12) Sokmen, M.; Candan, F.; Sumer, Z. *J. Photochem. Photobiol. A* **2001**, *143*, 241−244.

(13) Sunada, K.; Kikuchi, Y.; Hashimoto, K.; Fujishima, A. *Env. Sci. Technol.* **1998**, *32*, 726−728.

(14) Placer, Z. A.; Cushman, L. L.; Jonson, B. C. *Anal. Biochem.* **1966**, *16*, 359−364.

(15) Anderson, S. M.; Krinsky, N. I. *Photochem. Photobiol.* **1973**, *46*, 213−221.

(16) Blake, D.; Maness, P.; Huang, Z.; Wolfrum, E.; Huang, J.; Jacoby, W. *Sep. Purif. Methods* **1999**, *28*, 1−50.

(17) Dluhy, R.; Mendelsohn, R.; Casal, H. L.; Mantsch, H. H. *Biochemistry* **1983**, *22*, 1170−1177.

(18) Macpaill, R. A.; Strauss, H. L.; Snyder, R. G.; Elliger, C. A. *J. Phys. Chem.* **1984**, *88*, 334−341.

(19) Blume, A.; Hubner, W.; Messner, G. *Biochemistry* **1988**, *27*, 8239−8249.

(20) Lukes, P. J.; Yarwood, J. *Langmuir* **1992**, *8*, 3043−3050.

(21) Greenhall, M. H.; Yarwood, J.; Brown, R.; Swart, R. M. *Langmuir* **1998**, *14*, 2619−2626.

(22) Wolfangel, P.; Lehnert, R.; Meyer, H. H.; Muller, K. *Phys. Chem. Chem. Phys.* **1999**, *1*, 4833−4841.

(23) Cameron, N. D. G.; Mantsch, H. H. *Biophys. J.* **1982**, *38*, 175−184.

(24) Pohle, W.; Selle, C.; Rettig, W.; Heiser, U.; Dobner, B.; Wartewig, S. *Arc. Biochem. Biophys.* **2001**, *396*, 151−161.

(25) Dubois, J.; vandeVoort, F. R.; Sedman, J.; Ismail, A. A.; Ramaswamy, H. R. *J. Am. Oil Chem. Soc.* **1996**, *73*, 787−794.

(26) Levin, I. W.; Lewis, E. N. *Anal. Chem.* **1990**, *62*, 1101A−1111A.

(27) Nadtochenko, V.; Rincon, G. A.; Stanca, E. S.; Kiwi, J. J. *Photochem. Photobiol. Chem. A* **2004**, *169*, 131−137.